Applied Thermal Engineering 183 (2021) 116194

Contents lists available at ScienceDirect

Applied Thermal Engineering

journal homepage: www.elsevier.com/locate/apthermeng

Effects of C_2H_2 and C_2H_4 radiation on soot formation in ethylene/air diffusion flames

Shu Zheng [a], Yu Yang [a], Ran Sui [b], Qiang Lu [a,*]

[a] National Engineering Laboratory for Biomass Power Generation Equipment, North China Electric Power University, Beijing 102206, China
[b] Department of Mechanical and Aerospace Engineering, Princeton University, Princeton, NJ 08544, USA

ARTICLE INFO

Keywords:
Radiation
SNBCK
Soot formation
Ethylene flame

ABSTRACT

The involvement of hydrocarbons such as C_2H_4 and its combustion intermediate species C_2H_2 in thermal radiation has not been accounted in the numerical simulations of literature studies, which may in turn cause errors in estimating the soot formation processes. Numerical calculations were conducted using detailed gas-phase chemistry and thermal and transport properties in laminar coflow ethylene/air diffusion flames. The SNBCK model parameters for C_2H_2 and C_2H_4 were generated based on HITRAN database. The results show that the position of soot formation is affected by the radiation absorption of C_2H_4 at low temperatures and the radiation emission of C_2H_2 at high temperatures. The maximum C_2H_2/C_2H_4 radiation effect is 9.46% for air condition case and 9.87% for oxygen-enriched case. The height corresponding to the maximum soot volumetric fraction increases for the air condition while it decreases for the oxygen-enriched condition when the radiation effect is considered. The calculations reproduced well the experimental data of soot volumetric fraction in the literature and the numerical results were improved by 10.4% when considering the C_2H_2/C_2H_4 radiation. The results indicate that the radiation heat transfer of C_2H_2 and C_2H_4 needs to be taken into account in the numerical modeling of the ethylene/air diffusion flames.

1. Introduction

Gas thermal radiation plays an important role in the heat transfer and soot formation of combustion systems [1]. Due to the difficulty in solving the radiative transfer equation (RTE) in multidimensional geometry and the hyperspectral dependence of the absorption coefficient on the radiation gas [2–5], it is challenging to calculate the heat radiation transfer accurately and efficiently.

Ethylene laminar diffusion flame is a canonical problem in the study of radiation heat transfer in flames, because of its simple chemistry, moderate soot formation, and suitability for experiments under laboratory conditions [6,7]. Kaplan et al. [8] first considered radiation effects of soot, H_2O and CO_2 on the soot formation in ethylene diffusion flames. Liu et al. [9,10] studied the radiation heat transfer in counterflow and coflow ethylene laminar diffusion flames based on a detailed chemical reaction mechanism, a soot model and the statistical narrow-band correlated-*k* (SNBCK) model. They found the peak soot volumetric fraction increased by 8% when the gas radiation was ignored, and the radiation effect on soot nucleation and growth was larger than that on soot oxidation [10]. Subsequently, Guo and Smallwood [11,12] added CO_2 and H_2 in ethylene/air laminar diffusion flames to study the chemical and radiation effect of CO_2 and H_2 on soot inception and surface growth rates. However, the role of ethylene (C_2H_4) and its combustion intermediate species acetylene (C_2H_2) in thermal radiation has not been considered in the numerical simulations of ethylene flames, which may lead to errors in the predictions of soot formation. Guo et al. [13] studied the fuel preheating effect on soot formation and considered the radiative heat transfer of soot, H_2O, CO_2 and CO in two-dimensional coflow ethylene laminar diffusion flames. The results showed that the maximal C_2H_2 and C_2H_4 mole fractions were 0.084 and 1.0, respectively, while the maximal CO mole fraction was 0.088, indicating that the radiation absorption of C_2H_2 and C_2H_4 cannot be ignored. In recent years, several studies on [14–16] the radiation absorption effect of hydrocarbon fuels in combustion have been performed. De Ris [17] first pointed out that the effect of radiative heat transfer from combustion products to the fuel surfaces exceeded the conductive heat transfer in pool fires. To quantify the radiation absorption effect of fuel on determining the mass consumption rate in pool fires, Brosmer et al. [18] proposed a two-region flame model to predict the radiative flame feedback. However, detailed spectrally resolved radiation absorption properties for

* Corresponding author.
E-mail address: qianglu@mail.ustc.edu.cn (Q. Lu).

https://doi.org/10.1016/j.applthermaleng.2020.116194
Received 25 March 2020; Received in revised form 11 September 2020; Accepted 7 October 2020
Available online 13 October 2020

hydrocarbon fuels were missing in these studies.

To obtain the radiative characteristics of gases, the most straightforward way is the line-by-line (LBL) method [16], which however, requires numerous spectral line data and excessive computation time. In order to get higher computational efficiency, Chu [19] proposed the Planck mean absorption coefficients method for H_2O, CO_2, CO and CH_4 based on the LBL. This method does not need to solve the RTE but can be only used in optically thin cases. Since the radiative contribution of the mean absorption coefficient varies with the wavenumber, the narrow band models with low spectral resolution were proposed, such as the statistical narrow band (SNB) model [20–22], the spectral-line moment-based (SLMB) model [23] and the exponential wide-band (EWB) model. Soufiani et al. [24] generated narrow band (NB) parameters for H_2O, CO_2 and CO with a 25 cm^{-1} spectral resolution based on the HITEMP-2010 and CDSD-1000. To study pool fire radiation feedback, Consalvi et al. [25] established NB parameters for nine fuels (methane, methanol, ethane, ethylene, propane, propylene, heptane, methyl methacrylate and toluene) based on the NIST database. However, the narrow band models can be only used to obtain the gas transmissivity, which is suitable for solving the RTE in integral forms rather than differential forms. *k*-distribution methods can be used to obtain the gas absorption coefficient and are suitable for any RTE solver. Despite these previous studies, the *k*-distribution model for C_2H_2 and C_2H_4, and the radiation effect of hydrocarbon fuels in the soot formation have never been investigated.

The goal of this study was to numerically investigate the radiation effects of C_2H_2 and C_2H_4 on the soot formation in a laminar coflow ethylene/air diffusion flame at atmospheric pressure. First, the SNBCK model parameters for C_2H_2 and C_2H_4 were generated based on the HITRAN 2016 database. Subsequently, temperature, soot volumetric fraction, radiative source and soot growth rate distributions at four different cases when considering the radiation effects of C_2H_2 and C_2H_4 were evaluated and discussed. Finally, the simulation results were compared with experimental data.

2. Numerical model and validation

The flame code used in this study has been documented by Zhang [26] and described in details in several previous studies [27–29]. The Navier-Stokes equations and transport equations for low Mach numbers are solved in a 2D axisymmetric domain to obtain the distributions of mass, momentum, energy, gas-phase component, soot mass fraction and number density. The equations are discretized and solved using the control volume method, and the pressure–velocity coupling is treated by the SIMPLE algorithm. The chemical reaction mechanism (101 species and 544 reactions) of Appel et al. [30] was used. The soot model employed in this study has been described in detail by Zhang et al. [31]. Soot inception is assumed to a result of the collision of two pyrene molecules (A4). Surface growth and oxidation are assumed to follow the HACA mechanism [30]. All parameters associated with the HACA mechanism are taken from [30] and the fraction of the reactive soot surface sites α = 0.004exp(10800/T) [32] is adopted in this study. The aggregation process of soot particles is modeled using a sectional aerosol dynamics model [31]. The sectional transport equations for soot aggregates and primary particles can be found in [31]. Soot nucleation rate is calculated by the collision rate of two pyrene molecules in the free-molecular regime, but enhanced by a factor of 2.2 due to van der Waals force [33]. PAH condensation on soot particles also contributes to the surface growth of soot. The radiative source in the energy conservation equation was solved by the discrete ordinates method (DOM) coupled with the SNBCK model for considering the radiative properties of H_2O, CO_2, CO, C_2H_2 and C_2H_4. The soot absorption coefficient $5.5f_v/\lambda$ developed by Hottel and Sarofim [34] based on the Rayleigh's theory and the refractive index of soot was used.

In the SNBCK model, the mean gas transmissivity in the SNB model can be expressed as the distribution function of the absorption coefficient $f(k)$ in the narrow band through Laplace transform. With the Malkmus statistical narrow band model, the $f(k)$ can be described as [35]:

$$f(k) = \frac{1}{2}k^{-3/2}(BS)^{1/2}exp\left[\frac{\pi B}{4}\left(2 - \frac{S}{k} - \frac{k}{S}\right)\right] \quad (1)$$

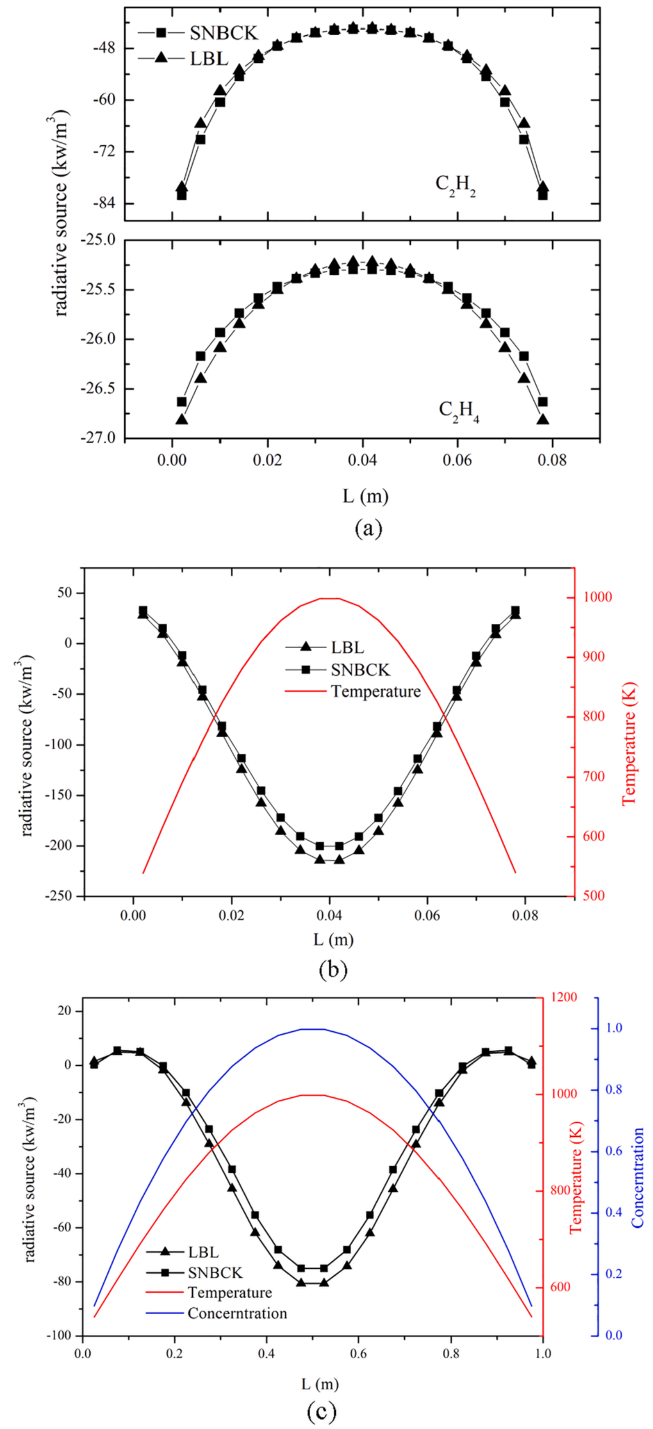

Fig. 1. Comparisons of radiative source calculated by SNBCK and LBL models for (a) $X_{C2H2} = 0.5$ at 1000 K in Case 1 and $X_{C2H4} = 0.5$ at 1000 K in Case 2; (b) a non-isothermal homogeneous gas mixture with temperature profile 500[1 + sin($\pi x/L$)] K, $X_{H2O} = 0.1$, $X_{CO2} = 0.1$, $X_{CO} = 0.05$, $X_{C2H2} = 0.05$ and $X_{C2H4} = 0.5$ in Case 3; (c) a non-isothermal inhomogeneous gas mixture with temperature profile 500[1 + sin($\pi x/L$)] K, $X_{H2O} = X_{C2H2} = X_{C2H4} = 4(1\text{-}x/L) \times x/L$ in Case 4.

Table 1
Flow conditions (unit L/min) of the ethylene laminar diffusion flames at air atmosphere.

Case	Air	Additional O_2	C_2H_4	O_2 volume fraction
1	240	–	0.194	0.21
2	240	–	0.150	0.21
3	75.9	44.1	0.194	0.5
4	91.1	28.9	0.194	0.4

where $B = 2\overline{\beta}_\eta/\pi^2$, $S = \overline{k}_\eta XP$ and $\overline{\beta}_\eta = 2\pi\overline{\gamma}_\eta/\overline{\delta}_\eta$. The SNB spectral parameters $\overline{\gamma}_\eta$, $\overline{\delta}_\eta$ and $\overline{k}_\eta$ for H_2O, CO_2 and CO developed by Soufiani [24] were used. The spectral range in this work is from 150 to 9300 cm^{-1} and the narrow bandwidth $\Delta\eta = 25$ cm^{-1}. The spectral line parameters for C_2H_2 and C_2H_4 are provided by HITRAN 2016. The narrow-band transmissivities of C_2H_2 and C_2H_4 calculated using the SNB and LBL models have been validated in Ref. [20]. C_2H_2 absorbs and emits radiation at all of the 367 narrow-bands while C_2H_4 has 52 radiating bands in the following two spectral regions: 675–1550 cm^{-1} (36 bands) and, 2900–3275 cm^{-1} (16 bands).

By introducing a cumulative function $g(k) = \int_0^k f(k')dk'$, Eq. (1) can be transformed to

$$g(k) = \frac{1}{2}[1 - erf(\frac{a}{\sqrt{k}} - b\sqrt{k})] + \frac{1}{2}[1 - erf(\frac{a}{\sqrt{k}} + b\sqrt{k})]e^{\pi B} \tag{2}$$

where $a = \sqrt{\pi BS}/2$, $b = \sqrt{\pi B/S}/2$ and $erf(x)$ is the error function $erf(x) = \frac{2}{\sqrt{\pi}}\int_0^x e^{-t^2}dt$. For each Gauss–Lobatto quadrature point g_i, the corresponding absorption coefficient $k_i = k(g_i)_\eta$ can be calculated iteratively by solving Eq. (2) using a combined Newton-Raphson and bisection method [36].

After getting the absorption coefficients of H_2O, CO_2, CO, C_2H_2, C_2H_4 and soot, the RTE can be solved by DOM. The discrete ordinates form of the RTE in a cylindrical coordinate system is [37]:

$$\frac{\mu_{m,l}}{r}\frac{\partial rI_{m,l}}{\partial r} - \frac{1}{r}\frac{\alpha_{m,l+1/2}I_{m,l+1/2} - \alpha_{m,l-1/2}I_{m,l-1/2}}{\omega_{m,l}} + \xi_{m,l}\frac{\partial I_{m,l}}{\partial z} = -k_{g(i)}\left(I_B - I_{m,l}\right) \tag{3}$$

where m is the polar angle, l the azimuth angle and, $\omega_{m,l}$ the quadrature weight.

Once the intensity field is calculated, the radiative source of each volume can be expressed as:

$$\nabla\cdot q = \sum_{i=1}^{N} w_i k_{g(i)}\left(4\pi I_B - \sum_{m=1}^{M}\sum_{l=1}^{L(m)}\omega_{m,l}I_{m,l}\right) \tag{4}$$

where N is the Gauss points and w_i the corresponding weight factor.

Model validations were conducted in four representative cases to assess the accuracy of the SNBCK model in predicting the absorption coefficients of C_2H_2 and C_2H_4. The thermal radiation heat transfer in a

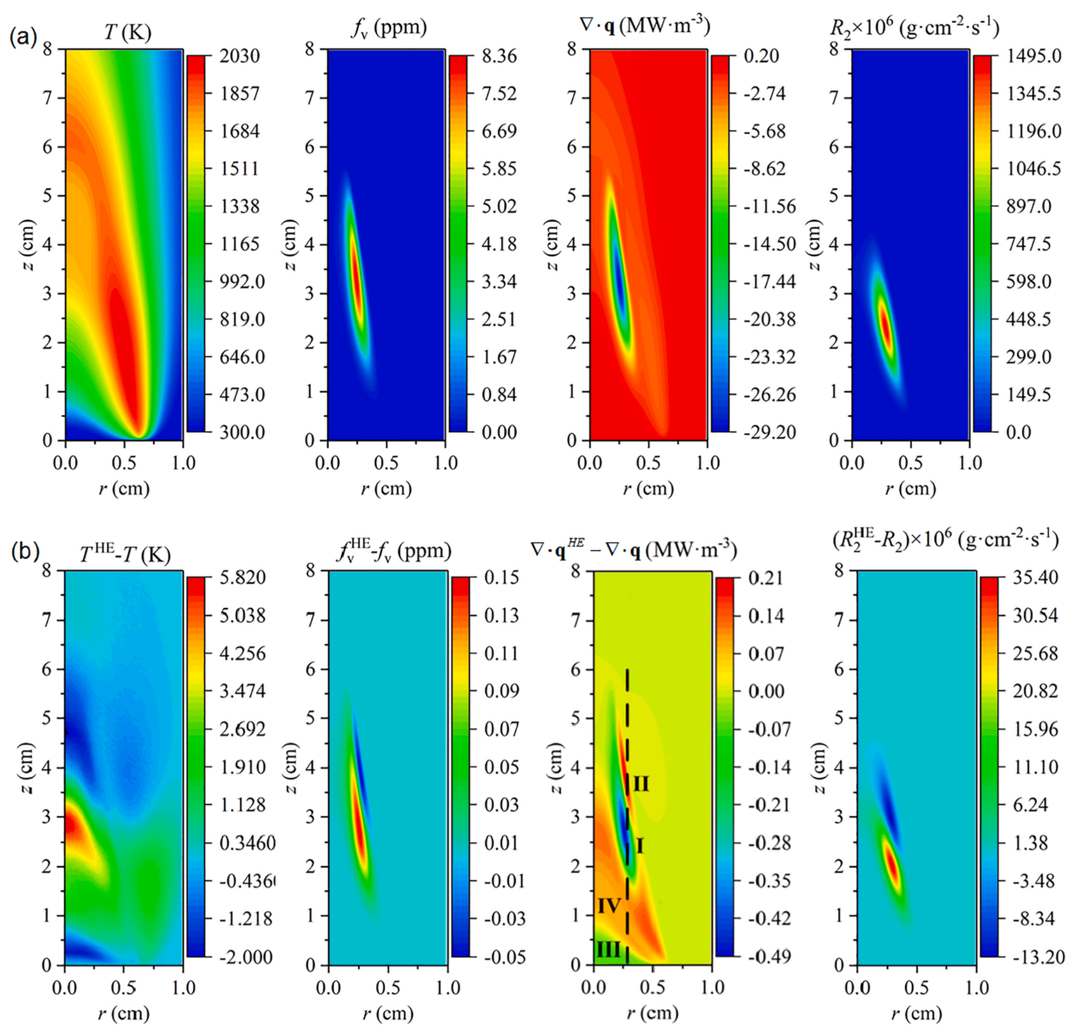

Fig. 2. (a) Distributions of the temperature T, soot volume fraction f_v, radiative source $\nabla\cdot q$and soot growth rate R_2 of Case 1; (b) distribution differences caused by the C_2H_2/C_2H_4 radiation effects in Case 1. Superscript HE denotes hydrocarbons excluded (i.e. without C_2H_2 and C_2H_4 radiation).

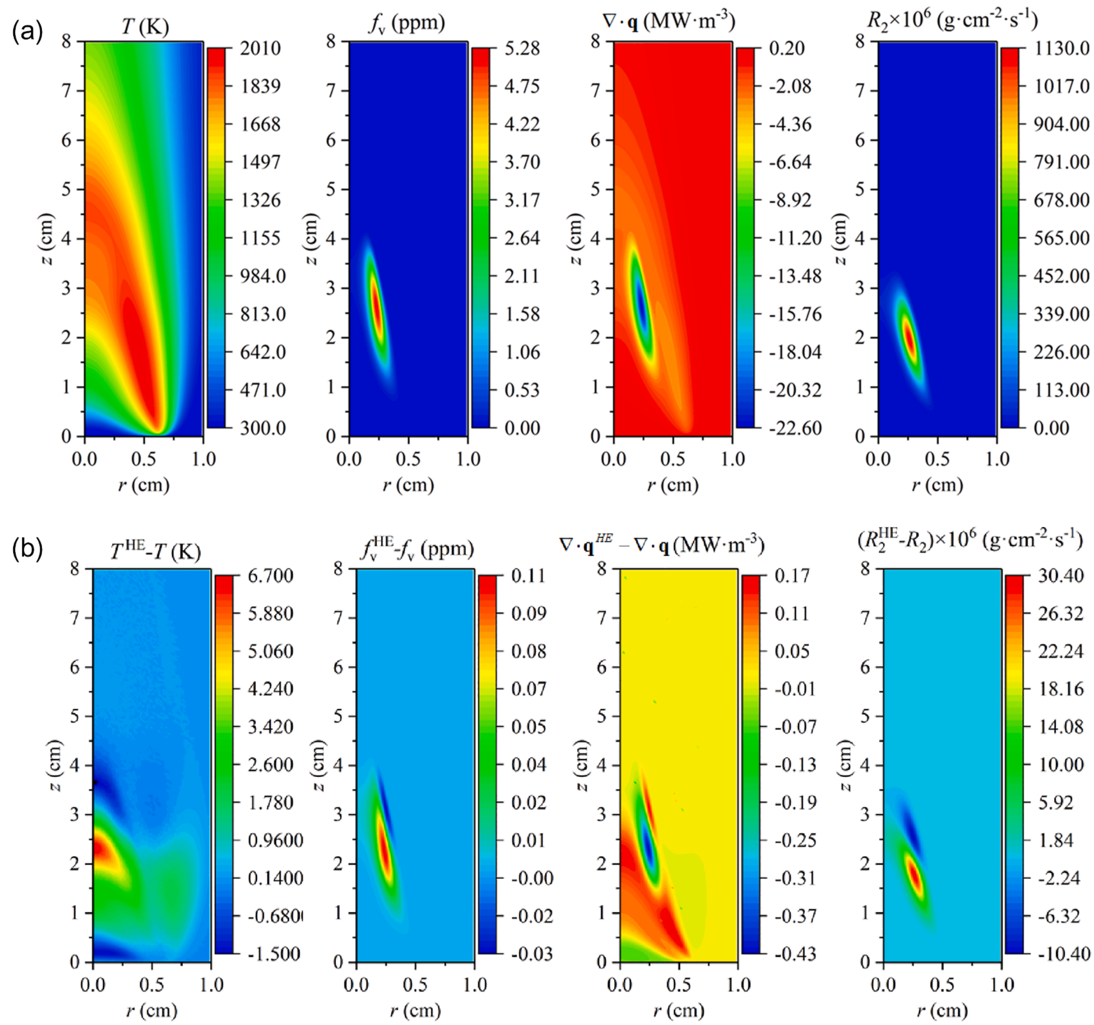

Fig. 3. (a) Distributions of the temperature T, soot volume fraction f_v, radiative source $\nabla\cdot q$ and soot growth rate R_2 of Case 2; (b) distribution differences caused by the C_2H_2/C_2H_4 radiation effects in Case 2. Superscript HE denotes hydrocarbons excluded (i.e. without C_2H_2 and C_2H_4 radiation).

one-dimensional planar slab was investigated and total pressure was fixed as 1 atm. These four cases contained an isothermal and homogeneous medium, non-isothermal homogeneous medium and non-isothermal inhomogeneous medium: $X_{C2H2} = 0.5$ at 1000 K in Case 1, $X_{C2H4} = 0.5$ at 1000 K in Case 2, the temperature of $500[1 + \sin(\pi x/L)]$ K, $X_{H2O} = 0.1$, $X_{CO2} = 0.1$, $X_{CO} = 0.05$, $X_{C2H2} = 0.05$ and $X_{C2H4} = 0.5$ in Case 3, the temperature of $500[1 + \sin(\pi x/L)]$ K, $X_{H2O} = X_{C2H2} = X_{C2H4} = 4(1\text{-}x/L) \times x/L$ in Case 4. The two slabs were diffusive black body with temperature 300 K. The parallel-plane space were segmented into 20 uniform volumes. As shown in Fig. 1, the comparisons between the LBL and SNBCK results show favorable agreements, illustrating the quality of the applied model parameter adjustments.

3. Results and discussion

Coflow laminar diffusion flames have been established by Gülder's burner [38] and were modeled in [27,32,39]. The fuel stream passes through the 10.9 mm inner diameter tube, while the air flow goes through an annular having the outer diameter of 88.7 mm. A non-uniform mesh with 332 × 87 control volumes (in the flow direction z and radial direction r, respectively) for the 15.353 × 6.0 cm^2 channel domain yielded grid-independent solutions. At the nozzle, the radial mesh length is 0.069 mm and the axial mesh length is 0.125 mm. The flow conditions of the four cases studied are summarized in Table 1. In Cases 1 and 2 air was used in the oxidizer flow, while Cases 3 and 4 had additional O_2 in air, i.e. "rich-oxygen conditions".

Fig. 2(a) shows the temperature, soot volumetric fraction, radiative source and soot growth rate distributions when considering the radiation effects of C_2H_2 and C_2H_4. The peak flame temperature was located in the annular region near the flame flank $r = 0.5$ cm, $z = 1$–3 cm, and the flame front was closed near the $z = 6$ cm. The peak soot volume fraction was located at $r = 0.25$ cm, $z = 2$–4 cm, since the soot is easy to generate at the fuel-enriched and high temperature region. The radiative source was affected by both distributions of temperature and soot volumetric fraction. The radiative source at the high soot volumetric fraction region is larger than that at the high temperature region, due to the stronger radiation capacity of soot than that of gaseous species. The soot growth rate distribution was similar to the acetylene concentration distribution (see Fig. 10 in [13]), except in the area near the axis where the soot growth rate is low caused by the less soot nucleation and lower temperature.

To facilitate discussions on the radiation effects of C_2H_2 and C_2H_4 in Fig. 2(b), the whole domain was categorized into four regimes based on the radiative source distributions: Regime I, $\nabla\cdot q < 0$, $\nabla\cdot q^{HE} - \nabla\cdot q < 0$ (radiative heat emission, the heat emission value decreased when considering the C_2H_2/C_2H_4 radiation); Regime II, $\nabla\cdot q < 0$, $\nabla\cdot q^{HE} - \nabla\cdot q > 0$ (radiative heat emission, the heat emission value increased when considering the C_2H_2/C_2H_4 radiation); Regime III, $\nabla\cdot q > 0$, $\nabla\cdot q^{HE} - \nabla\cdot q < 0$ (radiative heat absorption, the heat absorption value increased when considering the C_2H_2/C_2H_4 radiation); Regime IV,

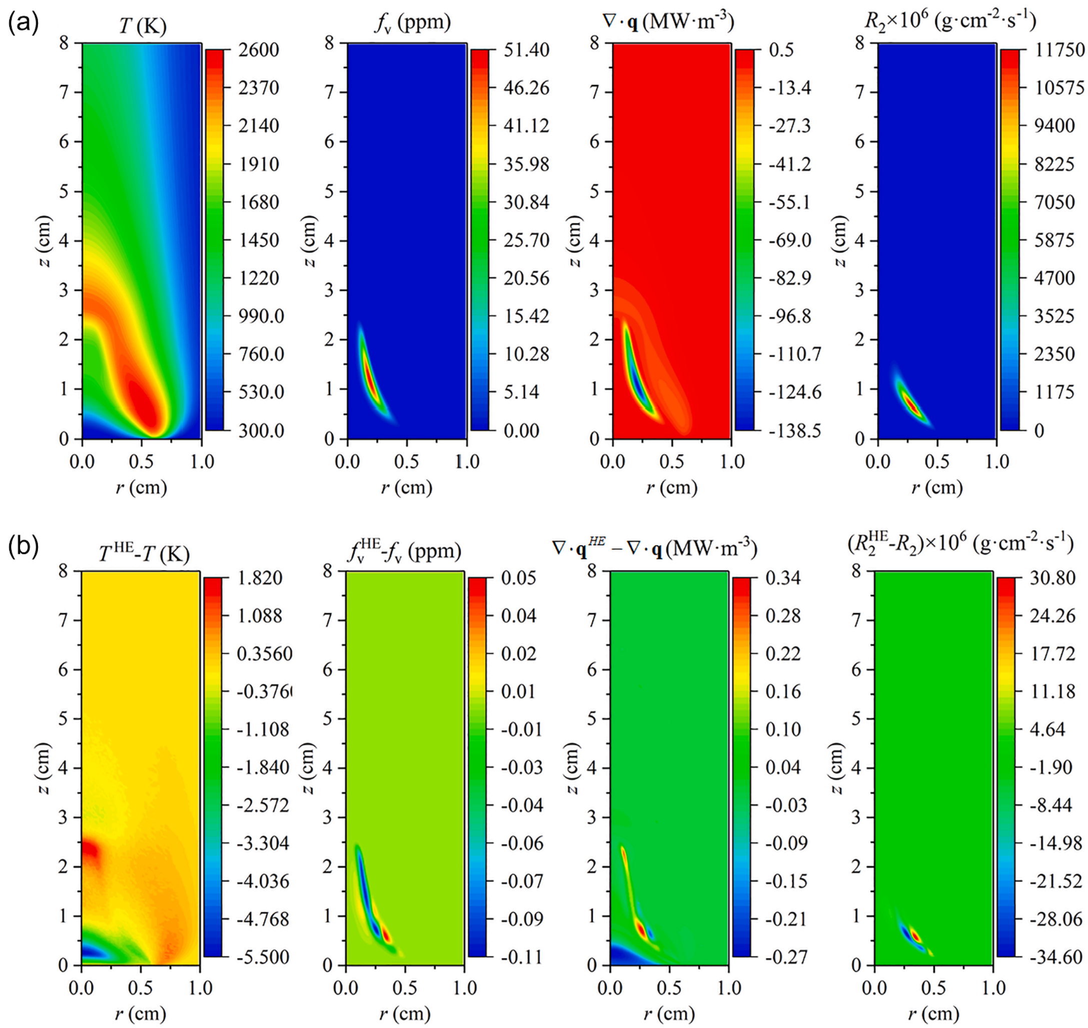

Fig. 4. (a) Distributions of the temperature T, soot volume fraction f_v, radiative source $\nabla\cdot q$ and soot growth rate R_2 of Case 3; (b) distribution differences caused by the C_2H_2/C_2H_4 radiation effects in Case 3.

$\nabla\cdot q > 0$, $\nabla\cdot q^{HE} - \nabla\cdot q > 0$ (radiative heat absorption, the heat absorption value decreased when considering the C_2H_2/C_2H_4 radiation).

As shown in Fig. 2(b), along the flow direction the radiative source $\nabla\cdot q$ in the burner outlet fell in Regime III. The predicted flame temperature decreased when the effects of C_2H_2/C_2H_4 radiation was absent due to fact that the high C_2H_4 concentration near the burner outlet absorbed radiation energy from the downstream burning area of the flame. Along the streamwise direction, Regime IV was realized downstream to Regime III. The reason is that the gas radiative emission energy increased with the rising C_2H_2 concentration and flame temperature. Subsequently, further downstream location along the dashed line fell in Regime I, where the flame temperature decreased when considering the effects of C_2H_2/C_2H_4 radiation due to the radiative heat loss to upstream locations of Regimes III and IV. As a result, the local soot formation was delayed and the radiative source decreased significantly at the same location in the presence of realistic C_2H_2/C_2H_4 radiation. Regime II was finally reached at the most downstream locations, where the radiative emission energy increased due to the delayed soot formation. This is also supported by the distributions of soot volumetric fraction f_v and soot growth rate R_2.

As shown in Fig. 3, Case 2 exhibited qualitatively similar distributions of gas temperature, soot volumetric fraction, radiative source and soot growth rate as Case 1. As the fuel flow rate of Case 2 was less than that of Case 1, the peak gas temperature and soot volumetric fraction in Case 2 were lower than those in Case 1. The maximum value of soot volumetric fraction is shown to move downward and inward in the spatial distribution caused by the reduced fuel flow rate.

To delineate the C_2H_2/C_2H_4 radiation effects at higher soot volumetric fraction, oxygen concentration in the oxidizer flows in Case 3 was increased by introducing additional O_2 in the air stream. As shown in Fig. 4(a), comparing to the Cases 1 and 2, the height of the flame decreased, while the soot was only distributed below 25 mm.

Fig. 4(b) shows that the flame temperature near the nozzle outlet was higher than that without considering the C_2H_2/C_2H_4 radiation effect. This difference was larger than in Case 1 due to its higher peak gas temperature and soot volume fraction. The difference of soot growth rate indicates that soot was more likely to form near the axis of symmetry ($r = 0$) when considering the C_2H_2/C_2H_4 radiation effect comparing to Cases 1 and 2. The reason was that the soot precursor concentration near the nozzle increased with the rising radiative absorption. Compared with Cases 1 and 2, the peak of radiative source difference ($\nabla\cdot q^{HE} - \nabla\cdot q$) moved from the high soot volumetric fraction region ($z \sim 2.5$ cm, see Fig. 2(b) and 3(b)) to the high C_2H_4 concentration region near the nozzle outlet. Moreover, the area of $\nabla\cdot q^{HE} - \nabla\cdot q > 0$ was larger than that of $\nabla\cdot q^{HE} - \nabla\cdot q < 0$ in Case 3 which was the opposite to Case 1 and 2, indicating stronger emission and weaker absorption. The reason was that the peak soot volumetric fraction increased when considering the C_2H_2/C_2H_4 radiation effect in the oxygen-enriched case.

Qualitatively similar to those of Case 3 but quantitatively lower

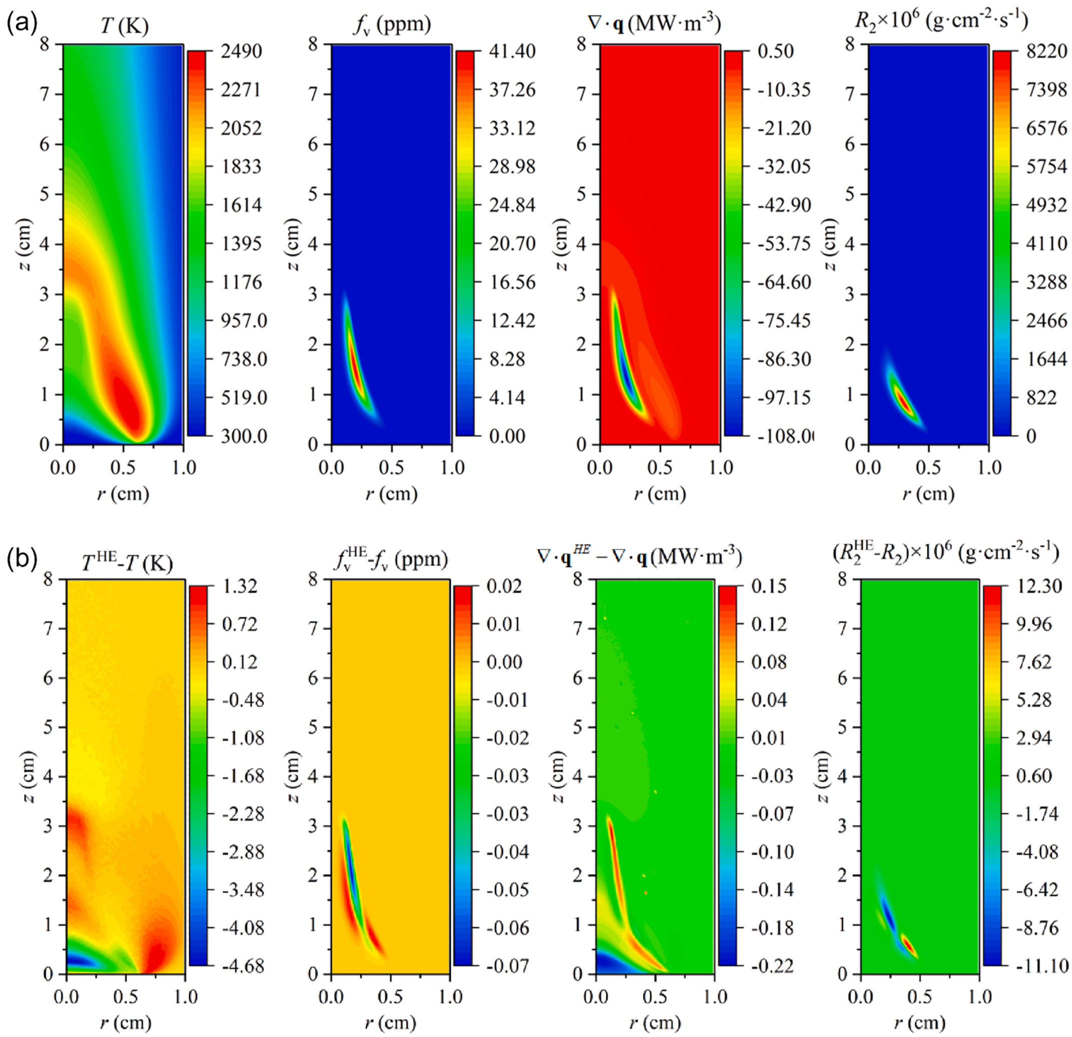

Fig. 5. (a) Distributions of the temperature T, soot volume fraction f_v, radiative source $\nabla \cdot q$ and soot growth rate R_2 of Case 4; (b) distribution differences caused by the C_2H_2/C_2H_4 radiation effects in Case 4. Superscript HE denotes hydrocarbons excluded (i.e. without C_2H_2 and C_2H_4 radiation).

temperatures and soot volumetric fraction distributions were obtained in Case 4 as shown in Fig. 5, due to the decreased oxygen addition into the air flow.

To quantitative analysis the C_2H_2/C_2H_4 radiation effect on the soot volume fraction, the relative changes of the soot volume fraction (f_v^{HE}-f_v)/f_v at main soot formation heights (z = 2.0, 2.5 and 3.0 cm for Case 1 and 2, z = 0.8, 1.0 and 1.2 cm for Case 3 and 4) were shown in Fig. 6. For Case 1 and 2, the maximum radiation effect was 9% at z = 2.5 cm and 9.46% at z = 2.0 cm, respectively. In the Fig. 6(a) and (b), the radiation effect showed positive first and then negative. For Case 3 and 4, the maximum radiation effect was 5.7% at z = 0.8 cm and 9.87% at z = 0.8 cm, respectively. In the Fig. 6(c) and (d), the radiation effect trend showed different from the Fig. 6(a) and (b), decreased first and then increased. The reason was that the soot formation was easier to happen near the axis of symmetry for oxygen-enriched cases which shown in Figs. 4 and 5.

However, the height corresponding to the maximum soot volumetric fraction was significantly affected by the radiation from C_2H_2 and C_2H_4, as summarized in Table 2. When the C_2H_2/C_2H_4 radiation effect was considered in the simulations, the height $Z_{max(fv)}$ corresponding to the maximum soot volumetric fraction increased by 3.04% and 1.88% in Cases 1 and 2, respectively. The reason was that the soot formation was delayed towards to the downstream direction and the overlapping region of soot formation and oxidation was enlarged by the effects of C_2H_2/C_2H_4 radiation. For Cases 3 and 4 at oxygen-enriched conditions, the height $Z_{max(fv)}$ corresponding to the maximum soot volumetric fraction decreased by 7.49% and 5.73%, respectively. This was caused by the change of temperature distribution, which moved the radial position of soot formation towards the axis of symmetry where C_2H_2 concentration was higher.

The calculated soot volumetric fractions considering the C_2H_2/C_2H_4 radiation effect and no C_2H_2/C_2H_4 radiation effect in Case 1 were compared to the experimental measurements reported by Liu et al. [40] and Snelling et al. [41]. The soot volume fractions measured by two-dimensional line-of-sight light attenuation (LOSA) corrected for scatter [41] were compared in Fig. 7.

Radial profiles of f_v at two selected heights are shown in Fig. 7. Experimental data was discarded at r < 1.5 mm due to the large measurement noise. It can be seen that the simulations considering the C_2H_2/C_2H_4 radiation effect well reproduced the profiles, especially the locations and peak values of soot volumetric fraction. When considering the C_2H_2/C_2H_4 radiation effect, the average relative errors were 13.4%, 12.1% and 25.4% at z = 2 cm, z = 3 cm and 4 cm. However, the average relative errors were 23.8%, 13.3% and 31.1% at z = 2 cm, z = 3 cm and 4 cm for no C_2H_2/C_2H_4 radiation effect. Therefore, the simulation results were improved by 10.4% at z = 2 cm in the flame of Case 1 when considering the C_2H_2/C_2H_4 radiation.

Apart from the dominating oxidative pyrolysis in non-premixed jet flames, other important reactions affecting C_2H_2 concentration were finally identified via the sensitivity analysis (SA) in a homogeneous

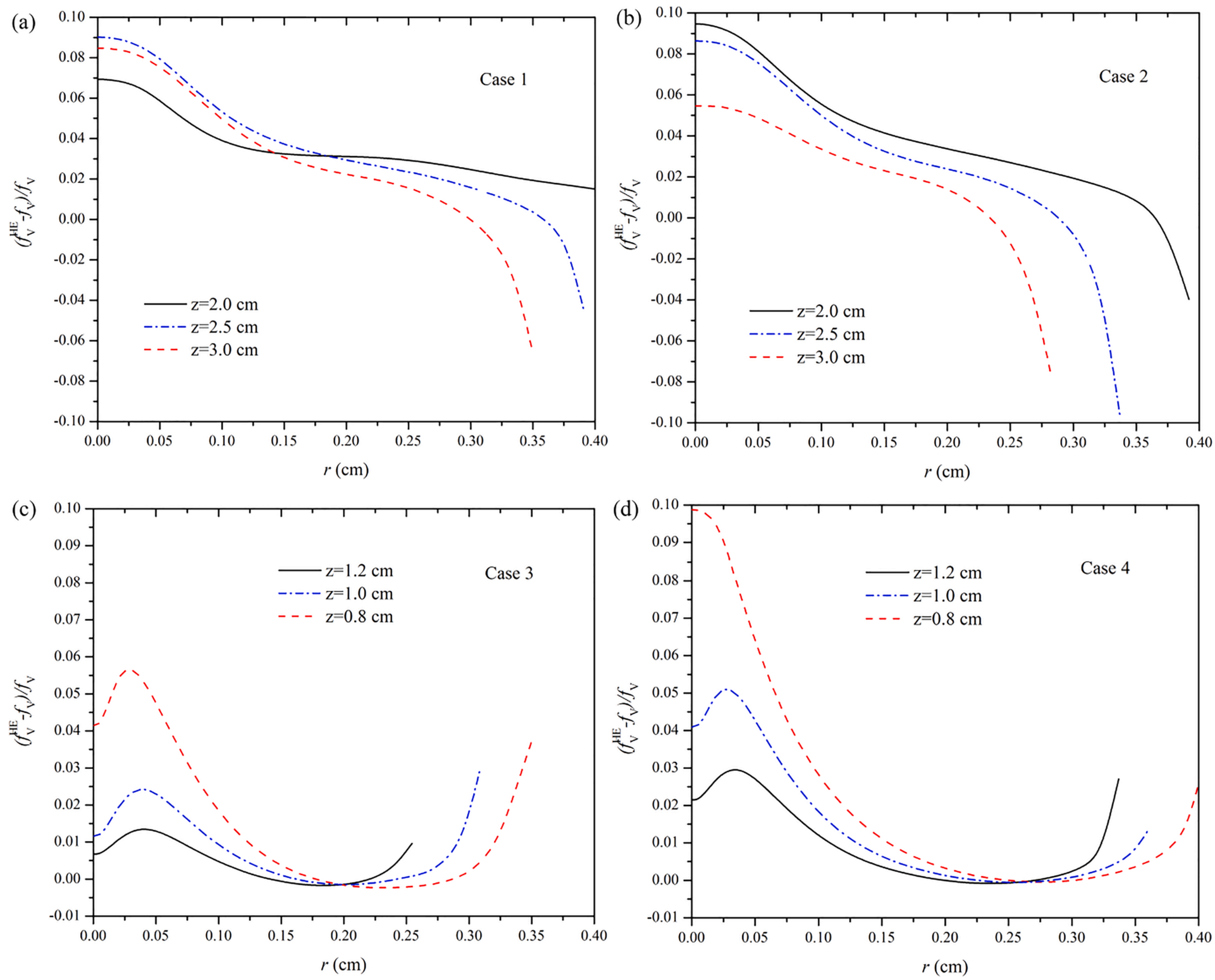

Fig. 6. C_2H_2/C_2H_4 radiation effect on the soot volume fraction (a) Case 1; (b) Case 2; (c) Case 3; (d) Case 4.

Table 2
The C_2H_2/C_2H_4 radiation effect on the height $Z_{max(fv)}$ corresponding to the maximum soot volumetric fraction.

Case	1	2	3	4
$Z_{max(fv)}$ (cm)	3.29	2.60	1.17	1.51
$Z_{max(fv)}^{HE}/Z_{max(fv)}$-1	−3.04%	−1.88%	7.49%	5.73%

system as shown in Fig. 8. The two controlling reactions were C_2H_2 reactions with O radical, i.e. $C_2H_2 + O = CH_2 + CO$ and $C_2H_2 + O = HCCO + H$ with negative sensitivity coefficients and $C_2H_4 + OH = C_2H_3 + H_2O$ with a positive sensitivity coefficient. Therefore, the consumption of C_2H_2 is mainly dominated by the availability of O while OH plays an important role in C_2H_2 formation.

4. Conclusions

A numerical study was conducted to investigate the radiation effects of C_2H_2 and C_2H_4 on soot formation in a laminar coflow ethylene/air diffusion flame at atmospheric pressure. The SNBCK model parameters for C_2H_2 and C_2H_4 were generated from SNB calculations based on the HITRAN 2016 database and were validated by the LBL method. The simulations well reproduced the literature experimental data of soot

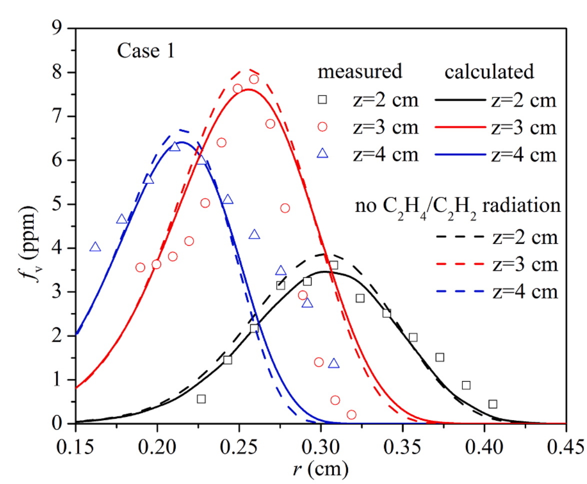

Fig. 7. Soot volumetric fraction f_v profiles as a function of radial location in the flame of Case 1 at height of 2 cm and 4 cm compared with hyperspectral imaging results in [40] and the height of 3 cm compared with two-dimensional LOSA scatter-corrected soot volume fractions in [41].

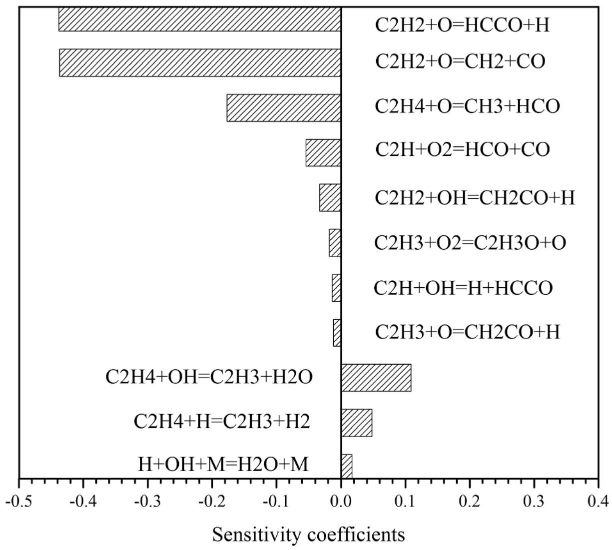

Fig. 8. Sensitivity coefficients of C_2H_2 concentration in a perfectly stirred reactor for C_2H_4/air flame.

volumetric fraction. The present results revealed that the position of soot formation was affected by the temperature distribution when considering the C_2H_2/C_2H_4 radiation, due to the radiation absorption of C_2H_4 at low temperatures and the radiation emission of C_2H_2 at high temperatures. When considering the C_2H_2/C_2H_4 radiation, for air conditions the height corresponding to the maximum soot volumetric fraction increased because the overlapping region of soot formation and oxidation was enlarged, while for oxygen-enriched conditions the height corresponding to the maximum soot volumetric fraction decreased as a result of soot formation shift towards the axis of symmetry where C_2H_2 concentration was higher. C_2H_2 concentration was mainly dominated by radical O and OH radicals as revealed by sensitivity analyses.

Declaration of Competing Interest

The authors declare that they have no known competing financial interests or personal relationships that could have appeared to influence the work reported in this paper.

Acknowledgements

This research was supported by the National Key Research Development Program of China (No.2017YFB0601900), the National Natural Science Foundation of China (No. 51976057, 51922040 and 51827808) and the Fundamental Research Funds for the Central Universities (No. 2020DF01).

References

[1] J.J. López, J.M. García-Oliver, A. García, D. Villalta, Development of a soot radiation model for diesel flames, Appl. Therm. Eng. 157 (2019), 113710.
[2] W. Fuqiang, W. Hao, G. Dayang, C. Ziming, M. Lanxin, Radiative transfer analysis of semitransparent medium with particles having non-uniform size distribution by differential-integration method, Int. J. Heat Mass Transf. 130 (2019) 342–355.
[3] Y. Liu, G. Liu, F. Liu, J.-L. Consalvi, Effects of the K-value solution schemes on radiation heat transfer modelling in oxy-fuel flames using the full-spectrum correlated K-distribution method, Appl. Therm. Eng. 170 (2020), 114986.
[4] F. Wang, X. Shi, C. Zhang, Z. Cheng, X. Chen, Effects of non-uniform porosity on thermochemical performance of solar driven methane reforming, Energy 191 (2020), 116575.
[5] S. Zheng, R. Sui, Y. Yang, Y. Sun, H. Zhou, Q. Lu, An improved full-spectrum correlated-k-distribution model for non-gray radiative heat transfer in combustion gas mixtures, Int. Commun. Heat Mass Transfer 114 (2020), 104566.
[6] W. Yan, S. Zheng, H. Zhou, Experiments investigation on 2D distribution of soot temperature and volume fraction by image processing of visible radiation, Appl. Therm. Eng. 124 (2017) 1014–1022.
[7] S. Zheng, Y. Yang, X. Li, H. Liu, W. Yan, R. Sui, Q. Lu, Temperature and emissivity measurements from combustion of pine wood, rice husk and fir wood using flame emission spectrum, Fuel Process. Technol. 204 (2020), 106423.
[8] C.R. Kaplan, S.W. Baek, E.S. Oran, J.L. Ellzey, Dynamics of a strongly radiating unsteady ethylene jet diffusion flame, Combust. Flame 96 (1994) 1–21.
[9] F. Liu, H. Guo, G.J. Smallwood, M. El Hafi, Effects of gas and soot radiation on soot formation in counterflow ethylene diffusion flames, J. Quant. Spectrosc. Radiat. Transfer 84 (2004) 501–511.
[10] F. Liu, H. Guo, G.J. Smallwood, Ö.L. Gülder, Effects of gas and soot radiation on soot formation in a coflow laminar ethylene diffusion flame, J. Quant. Spectrosc. Radiat. Transfer 73 (2002) 409–421.
[11] H. Guo, F. Liu, G.J. Smallwood, Ö.L. Gülder, Numerical study on the influence of hydrogen addition on soot formation in a laminar ethylene–air diffusion flame, Combust. Flame 145 (2006) 324–338.
[12] H. Guo, G.J. Smallwood, A numerical study on the influence of CO2 addition on soot formation in an ethylene/air diffusion flame, Combust. Sci. Technol. 180 (2008) 1695–1708.
[13] H. Guo, F. Liu, G.J. Smallwood, O.L. Gulder, The flame preheating effect on numerical modelling of soot formation in a two-dimensional laminar ethylene-air diffusion flame, Combust. Theor. Model. 6 (2002) 173–188.
[14] Q. Binauld, P. Rivière, A. Soufiani, A note on radiation preheating of some hydrocarbons by combustion products, Combust. Flame 194 (2018) 128–134.
[15] Minghou Xu, Dunxi Yu, Hong Yao, Xiaowei Liu, Yu Qiao, Coal combustion-generated aerosols: formation and properties, Proc. Combust. Inst. 33 (1) (2011) 1681–1697.
[16] S. Zheng, W. Liang, H. Chu, H. Zhou, Effects of radiation reabsorption of C1–C6 hydrocarbon flames at normal and elevated pressures, Fuel 266 (2020), 117061.
[17] J.D. Ris, Fire radiation—A review, Symposium on Combustion 17 (1979) 1003–1016.
[18] M.A. Brosmer, C.L. Tien, Radiative Energy Blockage in Large Pool Fires, Combust. Sci. Technol. 51 (1987) 21–37.
[19] Huaqiang Chu, Mingyan Gu, Huaichun Zhou, F. Liu, Calculations of narrow-band transimissities and the Planck mean absorption coefficients of real gases using line-by-line and statistical narrow-band models, Front. Energy 8 (2014) 41–48.
[20] C. Qi, S. Zheng, H. Zhou, Calculations of thermal radiation transfer of C2H2 and C2H4 together with H2O, CO2, and CO in a one-dimensional enclosure using LBL and SNB models, J. Quant. Spectrosc. Radiat. Transfer 197 (2017) 45–50.
[21] S. Zheng, C. Qi, Z. Huang, H. Zhou, Non-gray radiation study of gas and soot mixtures in one-dimensional planar layer by DRESOR, J. Quant. Spectrosc. Radiat. Transfer 217 (2018) 425–431.
[22] S. Zheng, Y. Yang, H. Zhou, The effect of different HITRAN databases on the accuracy of the SNB and SNBCK calculations, Int. J. Heat Mass Transf. 129 (2019) 1232–1241.
[23] Y. Sun, S. Zheng, B. Jiang, J. Tang, F. Liu, One-dimensional P1 method for gas radiation heat transfer in spherical geometry, Int. J. Heat Mass Transf. 145 (2019), 118777.
[24] P. Rivière, A. Soufiani, Updated band model parameters for H2O, CO2, CH4 and CO radiation at high temperature, Int. J. Heat Mass Transf. 55 (2012) 3349–3358.
[25] J. Consalvi, F. Liu, A database of narrow-band parameters for fuels commonly encountered in fire applications, Fire Saf. J. 78 (2015) 202–218.
[26] Q. Zhang, Detailed modeling of soot formation/oxidation in laminar coflow diffusion flames, Ph.D. thesis, University of Toronto, 2009.
[27] A. Fuentes, R. Henríquez, F. Nmira, F. Liu, J.-L. Consalvi, Experimental and numerical study of the effects of the oxygen index on the radiation characteristics of laminar coflow diffusion flames, Combust. Flame 160 (2013) 786–795.
[28] F. Liu, X. He, X. Ma, Q. Zhang, M.J. Thomson, H. Guo, G.J. Smallwood, S. Shuai, J. Wang, An experimental and numerical study of the effects of dimethyl ether addition to fuel on polycyclic aromatic hydrocarbon and soot formation in laminar coflow ethylene/air diffusion flames, Combust. Flame 158 (2011) 547–563.
[29] F. Liu, A.E. Karataş, Ö.L. Gülder, M. Gu, Numerical and experimental study of the influence of CO2 and N2 dilution on soot formation in laminar coflow C2H4/air diffusion flames at pressures between 5 and 20 atm, Combust. Flame 162 (2015) 2231–2247.
[30] J. Appel, H. Bockhorn, M. Frenklach, Kinetic modeling of soot formation with detailed chemistry and physics: laminar premixed flames of C2 hydrocarbons, Combust. Flame 121 (2000) 122–136.
[31] Q. Zhang, H. Guo, F. Liu, G. Smallwood, M. Thomson, Modeling of soot aggregate formation and size distribution in a laminar ethylene/air coflow diffusion flame with detailed PAH chemistry and an advanced sectional aerosol dynamics model, Proc. Combust. Inst. 32 (2009) 761–768.
[32] F. Liu, Y. Ai, W. Kong, Effect of hydrogen and helium addition to fuel on soot formation in an axisymmetric coflow laminar methane/air diffusion flame, Int. J. Hydrogen Energy 39 (2014) 3936–3946.
[33] F. Liu, J.-L. Consalvi, A. Fuentes, Effects of water vapor addition to the air stream on soot formation and flame properties in a laminar coflow ethylene/air diffusion flame, Combust. Flame 161 (2014) 1724–1734.
[34] H. Hottel, A. Sarofim, Radiative transport, McCravv Hill, New York, 1965.
[35] S. Zheng, R. Sui, W. Liang, H. Zhou, C.K. Law, On band lumping, radiation reabsorption, and high-pressure effects in laminar flame propagation, Combust. Flame 221 (2020) 86–93.
[36] F. Liu, G.J. Smallwood, O.L. Gulder, An accurate efficient and flexible SNBCK-based unified band model for calculations of spectrally resolved and integrated quantities in participating media containing real-gases, Heat Transfer 1 (2002) 663–668.
[37] H.-Y. Li, A two-dimensional cylindrical inverse source problem in radiative transfer, J. Quant. Spectrosc. Radiat. Transfer 69 (2001) 403–414.

[38] Ö. Gülder, D. Snelling, R. Sawchuk, in: Symposium (International) on Combustion, Elsevier, 1996, pp. 2351–2358.

[39] F. Liu, A.E. Karataş, Ö.L. Gülder, M. Gu, Numerical and experimental study of the influence of CO 2 and N 2 dilution on soot formation in laminar coflow C 2 H 4/air diffusion flames at pressures between 5 and 20atm, Combust. Flame 162 (2015) 2231–2247.

[40] H. Liu, S. Zheng, H. Zhou, Measurement of soot temperature and volume fraction of axisymmetric ethylene laminar flames using hyperspectral tomography, IEEE Trans. Instrum. Meas. 66 (2016) 315–324.

[41] D.R. Snelling, K.A. Thomson, G.J. Smallwood, M.L. Gülder, Two-dimensional imaging of soot volume fraction in laminar diffusion flames, Appl. Opt. 38 (1999) 2478–2485.